



UNIVERSITY OF LEEDS

This is a repository copy of *Oxidation products of biogenic emissions contribute to nucleation of atmospheric particles*.

White Rose Research Online URL for this paper:
<http://eprints.whiterose.ac.uk/80056/>

Version: Accepted Version

Article:

Riccobono, F, Schobesberger, S, Scott, CE orcid.org/0000-0002-0187-969X et al. (52 more authors) (2014) Oxidation products of biogenic emissions contribute to nucleation of atmospheric particles. *Science*, 344 (6185). pp. 717-721. ISSN 0036-8075

<https://doi.org/10.1126/science.1243527>

Reuse

Items deposited in White Rose Research Online are protected by copyright, with all rights reserved unless indicated otherwise. They may be downloaded and/or printed for private study, or other acts as permitted by national copyright laws. The publisher or other rights holders may allow further reproduction and re-use of the full text version. This is indicated by the licence information on the White Rose Research Online record for the item.

Takedown

If you consider content in White Rose Research Online to be in breach of UK law, please notify us by emailing eprints@whiterose.ac.uk including the URL of the record and the reason for the withdrawal request.



eprints@whiterose.ac.uk
<https://eprints.whiterose.ac.uk/>

Oxidation Products of Biogenic Emissions Contribute to Nucleation of Atmospheric Particles

5 Francesco Riccobono^{1§}, Siegfried Schobesberger², Catherine E. Scott³, Josef Dommen¹,
Ismael K. Ortega^{2†}, Linda Rondo⁴, João Almeida⁴, Antonio Amorim⁵, Federico Bianchi¹,
Martin Breitenlechner⁶, André David⁷, Andrew Downard⁸, Eimear M. Dunne^{3‡}, Jonathan
Duplissy², Sebastian Ehrhart⁴, Richard C. Flagan⁸, Alessandro Franchin², Armin Hansel⁶,
Heikki Junninen², Maija Kajos², Helmi Keskinen⁹, Agnieszka Kupc¹⁰, Andreas Kürten⁴,
10 Alexander N. Kvashin¹¹, Ari Laaksonen⁹, Katrianne Lehtipalo², Vladimir Makhmutov¹¹,
Serge Mathot⁷, Tuomo Nieminen^{2,12}, Antti Onnela⁷, Tuukka Petäjä², Arnaud P. Praplan¹,
Filipe D. Santos⁵, Simon Schallhart², John H. Seinfeld⁸, Mikko Sipilä^{2,12}, Dom V.
Spracklen³, Yuri Stozhkov¹¹, Frank Stratmann¹³, Antonio Tomé⁵, Georgios
Tsagkogeorgas¹³, Petri Vaattovaara⁹, Yrjö Viisanen¹⁴, Aron Vrtala¹⁰, Paul E. Wagner¹⁰,
Ernest Weingartner¹¹, Heike Wex¹³, Daniela Wimmer⁴, Kenneth S. Carslaw³, Joachim
15 Curtius⁴, Neil M. Donahue¹⁵, Jasper Kirkby⁷, Markku Kulmala^{2,12}, Douglas R. Worsnop^{2,16},
and Urs Baltensperger^{1*}

¹Paul Scherrer Institute, Laboratory of Atmospheric Chemistry, Villigen, Switzerland.

²University of Helsinki, Department of Physics, Helsinki, Finland.

20 ³University of Leeds, School of Earth and Environment, Leeds, United Kingdom.

⁴Goethe-University of Frankfurt, Institute for Atmospheric and Environmental Sciences, Frankfurt am Main, Germany.

⁵SIM, University of Lisbon and University of Beira Interior, Lisbon, Portugal.

⁶Ionic Analytik GmbH and University of Innsbruck, Institute for Ion and Applied Physics, Innsbruck, Austria.

⁷CERN, Geneva, Switzerland.

25 ⁸California Institute of Technology, Division of Chemistry and Chemical Engineering, Pasadena, California, USA.

⁹University of Eastern Finland, Kuopio, Finland.

¹⁰University of Vienna, Faculty of Physics, Vienna, Austria.

¹¹Lebedev Physical Institute, Solar and Cosmic Ray Research Laboratory, Moscow, Russia.

¹²Helsinki Institute of Physics, University of Helsinki, Helsinki, Finland.

30 ¹³Leibniz Institute for Tropospheric Research, Leipzig, Germany.

¹⁴Finnish Meteorological Institute, Helsinki, Finland.

¹⁵Carnegie Mellon University, Center for Atmospheric Particle Studies, Pittsburgh, PA, USA.

¹⁶Aerodyne Research Inc., Billerica, MA, USA.

[§]Present address: Joint Research Centre, European Commission, Ispra, Italy.

35 [†]Present address: Laboratoire de Physique des Lasers, Atomes et Molécules, Université de Lille 1, Villeneuve d'Ascq, France.

[‡]Present address: Finnish Meteorological Institute, Kuopio Unit, Kuopio, Finland.

[†]Present address: Institute for Aerosol and Sensor Technology, University of Applied Sciences, Windisch, Switzerland.

*Correspondence to: urs.baltensperger@psi.ch

40 **Abstract:**

Atmospheric new-particle formation affects climate and is one of the least understood atmospheric aerosol processes. The complexity and variability of the atmosphere has hindered elucidation of the fundamental mechanism of new-particle formation from gaseous precursors. Here we show, in experiments performed with the CLOUD chamber at

CERN, that sulfuric acid and oxidized organic vapors at atmospheric concentrations reproduce particle nucleation rates observed in the lower atmosphere. The experiments reveal a nucleation mechanism involving the formation of clusters containing sulfuric acid and oxidized organic molecules from the very first step. Inclusion of this mechanism in a
5 global aerosol model yields a photochemically and biologically driven seasonal cycle of particle concentrations in the continental boundary layer, in good agreement with observations.

Main Text:

10 Aerosol particles affect climate both directly by scattering and absorbing solar radiation and indirectly by acting as cloud condensation nuclei (CCN) (1). New-particle formation (nucleation) via gas-to-particle conversion is the largest source of atmospheric particles in the atmosphere (2) and it is thought to contribute up to half of the global CCN inventory (3, 4). It is therefore important to provide global models with accurate laboratory
15 measurements of nucleation rates as a function of the concentrations of vapor precursors in order to assess the impact of anthropogenic emissions (5).

Field measurements have shown that nucleation is strongly associated with the ambient vapor concentration of sulfuric acid (H_2SO_4), which is therefore considered to be a key component of atmospheric nucleation (6-9). Classical nucleation theories (CNT) of sulfuric
20 acid, water and ammonia are often used in global aerosol models (5). However, they grossly underestimate the ambient nucleation rates J observed in the planetary boundary layer (BL) at a given $[\text{H}_2\text{SO}_4]$ and overestimate the sensitivity of the nucleation rates to

[H₂SO₄] when compared with field observations (10, 11). This indicates that additional compounds participate in BL nucleation.

More recently, global aerosol models have shown improved estimation of the particle number concentration in the planetary boundary layer after the CNT nucleation rates were replaced with empirical parameterizations of field measurements using a power-law functional dependence of the form

$$J = k[\text{H}_2\text{SO}_4]^p \quad \text{Eq. 1}$$

where the exponent p ranges between 1 and 2 (7, 9, 11). The empirical pre-factor k varies by roughly a factor of 100 at different locations and times, reflecting the variability of the ambient parameters (such as temperature and ionization rates) but also the variability of other unaccounted compounds involved in atmospheric nucleation (7, 9). Oxidized biogenic organic vapors, ubiquitous in the boundary layer may well be important species involved in new-particle formation (7, 8, 12-15) but so far the identity of these additional chemical compounds - or class of compounds - remains unknown

Identification of the chemical composition of the nucleating clusters in field measurements is difficult, for several reasons. Vapor concentrations are extremely low (10^7 cm^{-3} or below) and the clusters contain only a few molecules. The presence of abundant “spectator” molecules and clusters in ambient air can obscure the actively-nucleating clusters. Empirical correlations such as the association of nucleation rates with H₂SO₄ are also strongly affected by the concurrent diurnal variations of other species, which are also formed via gas-phase photochemistry.

There is a paucity of studies demonstrating a quantitative overlap between ambient observations and laboratory measurements. Previous comparisons between laboratory experiments and ambient observations have mostly failed to reproduce ambient nucleation rates or to quantify their dependence on $[\text{H}_2\text{SO}_4]$ in the presence of pure sulfuric acid and water, or even with the addition of ammonia or organic compounds (16-22). A notable exception is the study by Chen et al. (23), showing reasonable agreement of predicted nucleation rates with rates measured in Atlanta and Mexico City when including efficient stabilization of the acids by bases such as amines (amine concentrations exceeded 100 pptv in Atlanta, but were not measured in Mexico City). Amines strongly enhance nucleation rates already in the low pptv range (24). Other studies included biogenic organic compounds but did not show direct evidence that organic compounds participate in the nucleation process itself, because they have been unable to distinguish between an effect of organics on nucleation or on the initial growth after nucleation has taken place (25, 26).

Zhang et al. investigated the enhancement of sulfuric acid nucleation in the presence of aromatic organic acids (17) or cis-pinonic acid (18), however, the stabilization of these organic compounds was lower than of those that are present during atmospheric nucleation, such that higher than ambient sulfuric acid concentrations were needed.

A critical limitation is that, until recently, nucleation rates were inferred by the appearance rate of particles at roughly 2 nm diameter. The appearance rate depends on the survival probability of nucleated particles growing to the observed size, which in turn depends strongly on their growth rate, making it difficult to disentangle nucleation and growth (27).

Thus there is a critical need for laboratory experiments that mimic the atmosphere under carefully controlled conditions.

We studied, under extraordinarily well-controlled laboratory conditions, nucleation in the presence of sulfuric acid and biogenic oxidized organic vapors, and at ionization rates and
5 vapor concentrations spanning atmospheric values. The CLOUD (Cosmics Leaving Outdoor Droplets) experiment at CERN provides a unique facility to measure the evolution from gas molecules to clusters to particles under atmospheric conditions. The CLOUD chamber is a 26 m³ stainless-steel vessel that enables nucleation experiments to be carried out under extremely stable, reproducible and essentially contaminant-free conditions (16); a
10 discussion of minute remaining contamination, which does not influence the measured nucleation rates, is given in the Supplementary Information (28). The gas and particle phases in the chamber are continuously sampled and analyzed by a comprehensive suite of state-of-the-art instruments (28). In these experiments, condensable vapors were formed by gas-phase reactions of hydroxyl radicals (OH), the dominant oxidant in the Earth's
15 atmosphere, with sulfur dioxide (SO₂) and pinanediol (PD, C₁₀H₁₈O₂). Sulfuric acid was formed from oxidation of SO₂, and a broad range of oxidized biogenic compounds was produced from oxidation of PD. Pinanediol is a first-generation oxidation product of α-pinene; consequently its oxidation products (in the following called BioOxOrg) closely represent later-generation oxidation products of biogenic monoterpenes. Based on the
20 experimental results, we developed a new parameterization describing the dependence of nucleation rates on [H₂SO₄] and [BioOxOrg] and implemented it in a global aerosol

microphysics model to assess the effect of this process on new-particle formation in the continental boundary layer.

The effects of H_2SO_4 and BioOxOrg on the nucleation rates were isolated by independently varying the concentration of $[\text{H}_2\text{SO}_4]$ or $[\text{BioOxOrg}]$ (see (28) for detailed experimental setup and $[\text{BioOxOrg}]$ determination). The CLOUD facility also benefits from an adjustable pion beam from the CERN Proton Synchrotron (PS) to simulate ionizing cosmic rays and from an electric clearing field of up to 20kV/m when an ion-free environment is needed. For each set of gas conditions we measured the nucleation rates J under three different ion concentrations: 1. J_n in an ion-free environment (“neutral”, with the electric field on); 2. J_{gcr} in a ground-level ionized environment (“gcr”, with ions naturally generated by galactic cosmic rays); 3. J_π in a typical high tropospheric environment (“pion beam”, provided by the CERN PS).

Figure 1A shows the measured nucleation rates at 1.7 nm mobility diameter ($J_{1.7}$). Despite the scatter due to associated uncertainties (mostly in the calculation of $[\text{BioOxOrg}]$), it is seen that at $[\text{BioOxOrg}] \geq 3 \times 10^6 \text{ cm}^{-3}$ the nucleation rates are similar to those observed in the ambient atmosphere (small squares in Fig. 1A) over the range of $[\text{H}_2\text{SO}_4]$ typically observed. At lower $[\text{BioOxOrg}]$ the $J_{1.7}$ values decrease, approaching those observed for nucleation from sulfuric acid either with water alone or with water and ammonia (green open markers in Figures 1A and 1B) (16).

Figures 1B and 1C show $J_{1.7}$ as a function of $[\text{H}_2\text{SO}_4]$ and $[\text{BioOxOrg}]$ with each other held nearly constant. For quasi-constant concentrations of BioOxOrg (~ 4 pptv, well within the atmospheric range) (14), we find the same power-law dependency on $[\text{H}_2\text{SO}_4]$ (Eq. 1) as

observed in field campaigns (marked area in Fig. 1B). The unconstrained least-squares fit (solid line) yields an exponent p with the corresponding 90% confidence interval of 2.17 ± 0.14 for the GCR conditions (green circles). Figure 1C shows that oxidized organic compounds contribute to $J_{1.7}$ at atmospheric H_2SO_4 mixing ratios (0.1 pptv). The unconstrained least-squares fit of $J = k[\text{BioOxOrg}]^q$ (solid line) yields an exponent q with the corresponding 90% confidence interval of 0.80 ± 0.23 for the GCR conditions (green circles).

Finally, Fig. 1D reveals the role of ions at atmospheric $[\text{H}_2\text{SO}_4]$ and $[\text{BioOxOrg}]$. It shows the percentage of the nucleation rate attributable to ions as a function of the total nucleation rate under GCR and pion beam conditions (shown in green and red, respectively). At lower-tropospheric GCR conditions the ion-induced fraction is about 60% at low nucleation rates ($J_{1.7} \leq 0.01 \text{ cm}^{-3} \text{ s}^{-1}$), falling to below 10% at high nucleation rates ($>10 \text{ cm}^{-3} \text{ s}^{-1}$). For upper-tropospheric ionization (pion beam conditions) the ion-induced fraction is about 10% higher than for GCR conditions. This decreasing ion contribution with increasing total nucleation rate (i.e. at higher $[\text{H}_2\text{SO}_4]$ and $[\text{BioOxOrg}]$) is consistent with an emerging picture that charge, bases, and oxidized organics all compete in stabilizing small H_2SO_4 clusters (16, 24). This picture suggests that ambient new-particle formation may involve any, or several, of these stabilizing agents, along with H_2SO_4 , depending on meteorological conditions and trace gas levels.

The dependence of J on $[\text{H}_2\text{SO}_4]$ and $[\text{BioOxOrg}]$ can be summarized in terms of a multicomponent power law

$$J = k_m [\text{H}_2\text{SO}_4]^p [\text{BioOxOrg}]^q \quad \text{Eq. 2}$$

where k_m is the multicomponent pre-factor. Nucleation occurs through a sequence of collisions between the growing clusters and vapor molecules where only a fraction of the BioOxOrg compounds are able to form stabilized clusters. We label the clusters with (n,m) where n and m correspond to the number of molecules of H_2SO_4 and BioOxOrg, respectively, present in the cluster. In the absence of coagulation or wall losses the survival probability of a cluster (n,m) will depend on the competition between its evaporation rate (which depends on the cluster composition) and the collision rate of the cluster with a condensable vapor molecule (which depends on the vapor concentration). A critical cluster is often defined to have a size at which it is equally likely to grow or to evaporate. According to the first nucleation theorem for multicomponent systems (29) the critical cluster composition is directly linked to the exponents p and q of Eq. 2.

However, the ‘critical cluster’ does not apply to systems where highly stabilized clusters are formed from the beginning: the slopes (exponents p and q of Eq. 2) are then defined by other, more important loss processes (i.e., the chamber walls in the CLOUD experiment or the pre-existing aerosol in the ambient atmosphere) (30). This also means that different conditions would yield different slopes. At very low condensing molecule concentrations, the time to reach 1.7 nm is increased and the wall loss or coagulation effects are accordingly enhanced (30), resulting in steeper slopes. At high concentrations, saturation effects similar to those found for amine concentrations (24) may be expected, resulting in shallower slopes or even complete saturation. Nevertheless, since our concentrations of H_2SO_4 and BioOxOrg are within the atmospheric range and since our condensation sink ($\sim 3 \times 10^{-3} \text{ s}^{-1}$) is similar to typical pristine boundary layer values (8), we conclude that our

slopes are representative of atmospheric nucleation. However this hypothesis will need to be tested in future experiments.

Confirmation that BioOxOrg compounds participate in nucleation from the very first step is provided by APi-TOF (atmospheric pressure interface time of flight) mass spectrometer data (28). Figure 2A shows an APi-TOF mass-defect plot where the deviation from the nominal (integer) mass (i.e., the “mass defect”) of a compound is plotted versus the exact mass (31). This plot reveals the molecular composition of the nucleating negatively charged clusters (up to ~ 1400 Th) and shows the presence of heteromers composed of various numbers of H₂SO₄ and BioOxOrg molecules (n,m), in addition to sulfuric acid monomers, dimers and trimers (red circles). Especially prominent are (1,1) (H₂SO₄, BioOxOrg) (yellow circles, 1st band), (2,1) (orange circles, 1st band), (1,2) and (2,2) (yellow and orange circles, respectively, 2nd band). These heteromers dominate the negative ion signals during the nucleation events. Pure sulfuric acid clusters above the trimer are absent. Several other mass-defect plots for different conditions are shown in the Supplementary Information (28).

The APi-TOF measurements confirm that the negatively charged clusters grow with time. Figure 2B shows the time series of the normalized cluster concentration of the four bands seen in Fig. 2A. The number m of the band corresponds to the number of BioOxOrg molecules present in the clusters of that band. The clusters additionally contain mainly one or two sulfuric acid molecules (one of which accommodating the negative charge by deprotonation to HSO₄⁻). Each new band appears with a delay of 3 to 10 minutes relative to the previous band, indicating that the clusters grow by the consecutive addition of BioOxOrg molecules. However, the preferential pathway for growing clusters will depend

on the collision and evaporation rates which in turn depend on the relative vapor concentrations, the oxidation state of the BioOxOrg molecules and the charge on the cluster. Figure 2B also shows the appearance of 2 and 3 nm particles, providing evidence that the nucleated clusters indeed grow into larger particles sequentially detected by particle
5 counters with higher cut-offs. It should be noted that the APi-TOF measured only negatively charged clusters, and the pathways for neutral clusters could be different. However, Schobesberger et al. (32) showed similar growth rates for charged and neutral clusters involving BioOxOrg molecules which explains the good agreement with the particle counters in Fig. 2B.

10 The large enhancement of the nucleation rate with BioOxOrg is due to the formation of clusters with much lower evaporation rates than those of binary sulfuric acid clusters. Quantum chemical calculations (28) indicate that the evaporation rate of a neutral sulfuric acid dimer is much higher than that of a highly oxidized BioOxOrg molecule clustered in a heterodimer with one sulfuric acid molecule (e.g. by a factor 10^4 for a 3-methyl-1,2,3-
15 butane-tricarboxylic acid molecule).

Notwithstanding the caveats on the slopes of the nucleation rates versus $[\text{H}_2\text{SO}_4]$ and $[\text{BioOxOrg}]$, which may vary with experimental conditions, we have parameterized these dependencies to investigate the resulting particle production in a global aerosol model. Setting $p = 2$ and $q = 1$ in Eq. 2 we obtain $k_m = 3.27 \times 10^{-21} \text{ cm}^6 \text{ s}^{-1}$ with 90% confidence
20 interval edges of 1.73×10^{-21} and $6.15 \times 10^{-21} \text{ cm}^6 \text{ s}^{-1}$. A nucleation rate in the form $J = k_m[\text{H}_2\text{SO}_4]^2[\text{BioOxOrg}]$ can be compared to rates in the form $J = k'[\text{H}_2\text{SO}_4]^2$ that have been fitted empirically to ambient measurements (7,9), which yield an effective pre-factor

k' that lies in the range $0.01-10 \times 10^{-12} \text{ cm}^3 \text{ s}^{-1}$. For example, with α -pinene mixing ratios of 200 pptv (e.g., (33)), a condensation sink rate of monomers of 10^{-3} s^{-1} and $[\text{OH}]=10^6 \text{ cm}^{-3}$, we estimate $k'=1.3 \times 10^{-12} \text{ cm}^3 \text{ s}^{-1}$, which is well within measured values (see 28). While both parameterizations are consistent with ambient observations (7, 9), our new
5 parameterization contains an explicit dependence on organics. The parameterized CLOUD data can thus be used to quantitatively test the hypothesis that organic-sulfuric acid nucleation plays an important role in the planetary boundary layer, with relatively few assumptions since the parameterization is based on laboratory measurements made under realistic, albeit limited, atmospheric conditions.

10 We included this parameterization in a three-dimensional global aerosol model, GLOMAP (34, 35). The concentration of BioOxOrg was calculated assuming it derives from a two-stage oxidation of α -pinene to first-generation products and then to BioOxOrg, with the α -pinene emitted from the terrestrial biosphere (36). The new parameterization resulted in a 57% (90% confidence interval range: 46 - 70%) increase in the global annual mean particle
15 (> 3 nm in diameter) number concentration in the boundary layer compared with a control simulation that included only binary homogenous nucleation, BHN (from a global annual mean value of 450 cm^{-3} for BHN to 706 cm^{-3} (range: $654 - 765 \text{ cm}^{-3}$) for the new parameterization). The increase in particle concentrations occurs mostly over land areas, where α -pinene is emitted; the mean fractional increase in particle number concentration is
20 97% (range: 78 – 119%) over land and 49% (range: 40 – 60%) over the ocean. In contrast, when the nucleation rate in the boundary layer is defined as $J=k_{\text{ACT}}[\text{H}_2\text{SO}_4]$ the enhancement is 79% over land and 137% over oceans, which is likely to be an unrealistic

marine/land contrast because it neglects the modulation caused by lower organic compound concentrations over remote marine regions.

Figure 3 shows the seasonal cycle in simulated and observed particle number concentrations across 19 locations in the northern hemisphere continental boundary layer (11); see (29) for further detail. Model simulations based on the assumption that only H_2SO_4 controls nucleation in the boundary layer ($J = k_{\text{ACT}}[\text{H}_2\text{SO}_4]$ with rate coefficients determined from ambient data as in Fig. 1A (7, 9)) tend to predict peak particle concentrations in early spring and autumn, with summer nucleation being suppressed by the higher condensation sink. Our new parameterization (dark green line in Figure 3) improves both the simulated magnitude and seasonal variation of particle concentration (Table S3), including the summer peak caused by the strong seasonal variation in biogenic emissions and $[\text{OH}]$ ($[\text{OH}]$ appears to the power of 3 in the experimentally determined rate since it accounts for the oxidation both of organics to BioOxOrg and of SO_2 to H_2SO_4). This difference in seasonality between $J = k_{\text{ACT}}[\text{H}_2\text{SO}_4]$ and our new mechanism is particularly apparent at sites located in or near forests (Table S3), but less apparent at polluted sites where biogenic emissions play a smaller role. At the forest sites, the mean correlation coefficient between the modeled and observed monthly mean concentrations is 0.7 using our new mechanism, but only 0.35 using $J = k_{\text{ACT}}[\text{H}_2\text{SO}_4]$, so the new mechanism can explain about 50% of the temporal variability in particle concentrations but activation nucleation can explain only 12%. The Metzger et al. (25) mechanism ($J = k_{\text{MET}}[\text{H}_2\text{SO}_4][\text{NucOrg}]$) also improves the seasonal cycle, but it is important to note that

it assumes that the anthropogenic organic compound used in those experiments is representative of α -pinene in the model, for which there is no evidence.

There are many other uncertain model processes that could control the seasonality of particle concentrations. However, in a model study sampling from the 28-dimensional uncertainty space of model processes and emissions (37; 38), the summer dip in particle concentrations was shown to be a robust feature of the model when nucleation is driven only by H_2SO_4 . This problem seems to be overcome here by including a biogenically controlled nucleation mechanism. Figure 3 shows a remaining model-observation bias in particle concentrations in winter, which may reflect other uncertain processes or emissions (37) or may indicate that other nucleation mechanisms are operating which are controlled by non-biogenic compounds. However, at present, there are no measurements that enable the competing effects of compounds like ammonia, amines and oxidized organics to be accounted for in a model.

Recent experimental results and quantum chemical calculations have shown that amines and ions can also effectively stabilize the sulfuric acid clusters, reducing evaporation rates and enhancing the nucleation rates at low $[\text{H}_2\text{SO}_4]$ (24, 39, 40). Thus the dominant nucleation pathway may ultimately depend on the local atmospheric concentration of H_2SO_4 , ions, amines and on the concentration and functionalization of BioOxOrg, all of which vary considerably over time and space. At present, these compounds cannot be combined in a single mechanism because of the unknown way in which they compete with each other to stabilize clusters. Challenging laboratory and field measurements, as well as accurate modeling, of all these variables are required to predict the dominant nucleation

pathway at different locations and eventually to understand the global effect of new-particle formation on climate. However, our model simulations show that the nucleation of sulfuric-acid and oxidized biogenic organic compounds (BioOxOrg) explains some features of the observed seasonal cycle of new particles in the continental boundary layer that cannot be explained by sulfuric acid alone. Along with the experimental evidence presented here, it appears that highly oxidized biogenic organic vapors and sulfuric acid together play a major role in new-particle formation in the boundary layer.

References and Notes:

1. IPCC, Climate Change 2007: the Physical Science Basis. Contribution of Working Group I to the Fourth Assessment Report of the Intergovernmental Panel on Climate Change, S. Solomon et al., Eds. (Cambridge Univ. Press, New York, 2007).
2. M. Kulmala et al., *J. Aerosol Sci.* **35**, 143 (2004).
3. F. Yu, G. Luo, *Atmos. Chem. Phys.* **9**, 7691 (2009).
4. J. Merikanto, D. V. Spracklen, G. W. Mann, S. J. Pickering, K. S. Carslaw, *Atmos. Chem. Phys.* **9**, 8601 (2009).
5. R. Y. Zhang, A. Khalizov, L. Wang, M. Hu, W. Xu, *Chem. Rev.* **112**, 1957 (2012).
6. R. J. Weber et al., *J. Geophys. Res.-Atmos.* **102**, 4375 (1997).
7. S. L. Sihto et al., *Atmos. Chem. Phys.* **6**, 4079 (2006).
8. I. Riipinen et al., *Atmos. Chem. Phys.* **7**, 1899 (2007).
9. C. Kuang, P. H. McMurry, A. V. McCormick, F. L. Eisele, *J. Geophys. Res.-Atmos.* **113**, D10209 (2008).
10. R. J. Weber et al., *Chem. Eng. Commun.* **151**, 53 (1996).
11. D. V. Spracklen et al., *Atmos. Chem. Phys.* **10**, 4775 (2010).
12. R. J. Weber et al., *J. Geophys. Res.-Atmos.* **103**, 16385 (1998).
13. F. L. Eisele et al., *J. Geophys. Res.-Atmos.* **111**, D04305 (2006).
14. P. Paasonen et al., *Atmos. Chem. Phys.* **10**, 11223 (2010).
15. M. Kulmala et al., *Science* **339**, 943 (2013).
16. J. Kirkby et al., *Nature* **476**, 429 (2011).
17. R. Y. Zhang et al., *Science* **304**, 1487 (2004).
18. R. Y. Zhang et al., *Proc. Natl Acad. Sci. USA* **106**, 17650, (2009).
19. S. M. Ball, D. R. Hanson, F. L. Eisele, P. H. McMurry, *J. Geophys. Res.-Atmos.* **104**, 23709 (1999).
20. L. H. Young et al., *Atmos. Chem. Phys.* **8**, 4997 (2008).
21. A. Laaksonen et al., *Atmos. Chem. Phys.* **8**, 7255 (2008).
22. A. Sorokin, F. Arnold, *Atmos. Environ.* **41**, 3740 (2007).
23. Chen, M. et al., *Proc. Natl Acad. Sci. USA* **109**, 18713 (2012).
24. J. Almeida et al., *Nature*, 502, 359 (2013).
25. A. Metzger et al., *Proc. Natl Acad. Sci. USA* **107**, 6646 (2010).
26. F. Riccobono et al., *Atmos. Chem. Phys.* **12**, 9427 (2012).
27. M. Sipila et al., *Science* **327**, 1243 (2010).
28. Materials and methods are available as supporting material on Science Online.

29. D. W. Oxtoby, D. Kashchiv, *J. Chem. Phys.* **100**, 7665 (1994).
30. S. Ehrhart, J. Curtius, *Atmos. Chem. Phys.* **13**, 11465 (2013).
31. M. Ehn et al., *Atmos. Chem. Phys.* **10**, 8513 (2010).
32. S. Schobesberger et al., *Proc. Natl Acad. Sci USA*, **110**, 17223 (2013)
- 5 33. H. Hakola, H. Hellen, M. Hemmila, J. Rinne, M. Kulmala, *Atmos. Chem. Phys.* **12**, 11665 (2012).
34. D. V. Spracklen, K. J. Pringle, K. S. Carslaw, M. P. Chipperfield, G. W. Mann, *Atmos. Chem. Phys.* **5**, 2227 (2005).
35. G. W. Mann et al., *Geosci. Model Dev.* **3**, 519 (2010).
36. A. Guenther et al., *J. Geophys. Res.-Atmos.* **100**, 8873 (1995).
- 10 37. L.A. Lee et al., *Atmos. Chem. Phys.* **13**, 8879 (2013).
38. K. S. Carslaw et al., *Faraday Discuss.* **165**, 495 (2013).
39. A. B. Nadykto, F. Q. Yu, *Chem. Phys. Lett.* **435**, 14 (2007).
40. T. Kurten, V. Loukonen, H. Vehkamäki, M. Kulmala, *Atmos. Chem. Phys.* **8**, 4095 (2008).

15

Acknowledgments:

We would like to thank CERN for supporting CLOUD with important technical and financial resources, and for providing a particle beam from the CERN Proton Synchrotron. We also thank J.-L. Agostini, P. Carrie, L.-

5 P. De Menezes, F. Josa, I. Krasin, R. Kestic, O.S. Maksumov, S.V. Mizin, R. Sitals, A.Wasem and M. Wilhelmsson for their important contributions to the experiment. We would like to acknowledge Chongai Kuang and Veli-Matti Kerminen for providing the observational datasets used in Figure 1A, and the authors that contributed to them. This research was funded by the EC 7th Framework Programme (Marie Curie Initial Training Network "CLOUD-ITN", grant no. 215072), the ERC Advanced Grant "ATMNUCLE" (no.

10 227463), the Academy of Finland via the Centre of Excellence programme (project no. 1118615) and grant no. 1133872, the German Federal Ministry of Education and Research (project no. 01LK0902A), the Swiss National Science Foundation (project nos. 206621_125025 & 206620_130527), the Austrian Science Fund (project nos. P19546 & L593), the Portuguese Foundation for Science and Technology (project no. CERN/FP/116387/2010), the Russian Foundation for Basic Research (grant N08-02-91006-CERN), the

15 Davidow Foundation, and the U.S. National Science Foundation (grants AGS1136479 and CHE1012293).

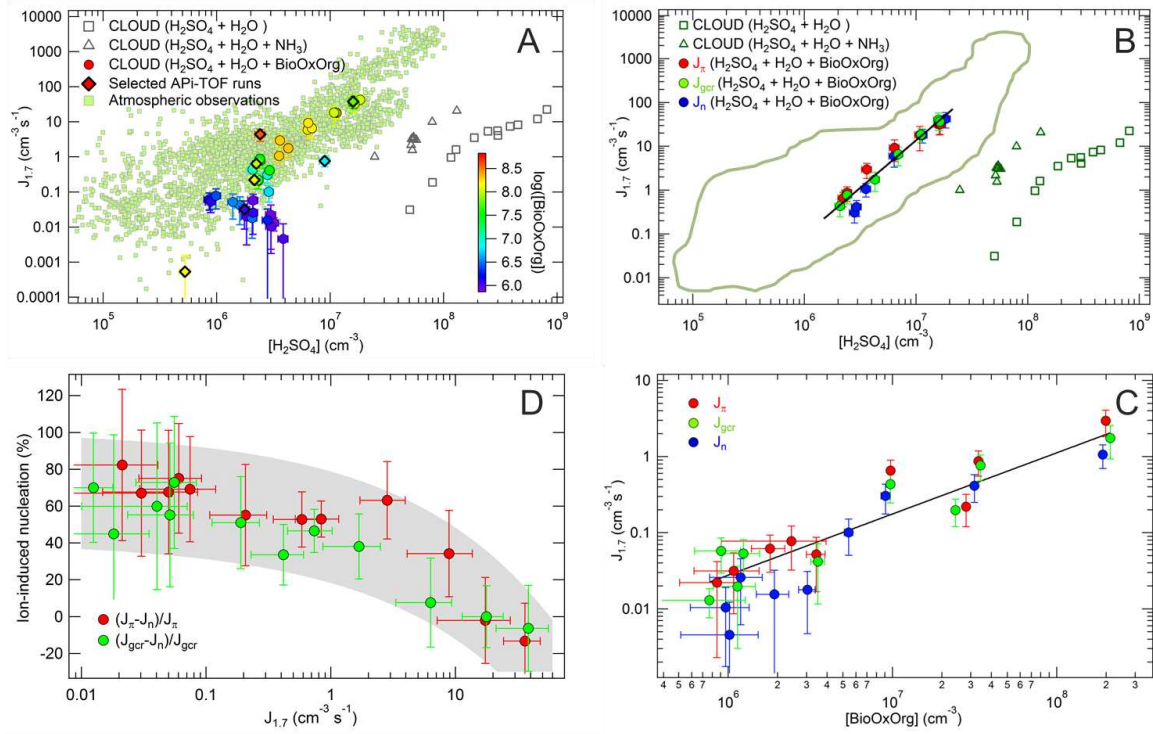


Figure 1. Clockwise from top left: (A) Nucleation rates $J_{1.7}$ as a function of $[H_2SO_4]$ for the whole range of $[BioOxOrg]$ experimentally explored (color coded with $\log[BioOxOrg]$), and nucleation rates observed in the boundary layer (small green squares) (7-9). Contaminants NH_3 and dimethylamine are < 2 pptv and < 1 pptv, respectively. Bold diamonds correspond to those runs for which the APi-TOF mass defect plots are shown in Figures 2, S2, S3 and S4. (B) Nucleation rates $J_{1.7}$ as a function of $[H_2SO_4]$ for a limited range of $[BioOxOrg]$ ($1.0 \pm 0.7 \cdot 10^8$ cm⁻³, ~ 4 pptv). The marked area represents the region of boundary layer observations. (C) Nucleation rates as a function of $[BioOxOrg]$ for a limited range of $[H_2SO_4]$ ($1.9 \pm 0.7 \cdot 10^6$ cm⁻³, ~ 0.1 pptv). (D) Percentage of ion-induced nucleation as a function of the total nucleation, calculated from the differences of the corresponding experiments under identical conditions. In (B), (C) and (D) blue, green and red circles correspond to J_n , J_{gcr} and J_π , respectively. The bars represent 1σ total errors, but the overall systematic scale uncertainty on $[H_2SO_4]$ (about factor 2) and $[BioOxOrg]$ is not shown. In (A) and (B) the binary (H_2SO_4 and H_2O , open squares) and ternary (H_2SO_4 , H_2O and NH_3 , open triangles) GCR nucleation rates from CLOUD are also shown (16). The black lines correspond to unconstrained least-squares fits for GCR conditions. The gray band in panel D is shown to guide the eye.

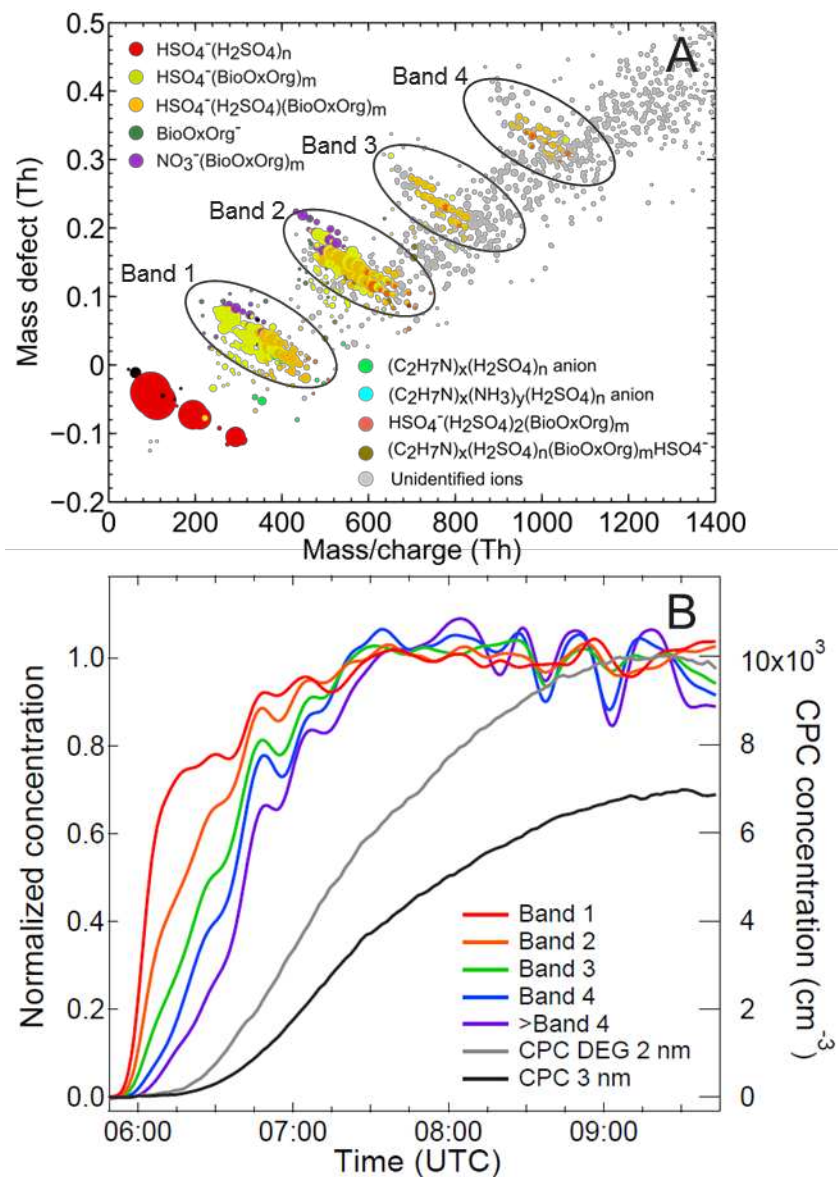
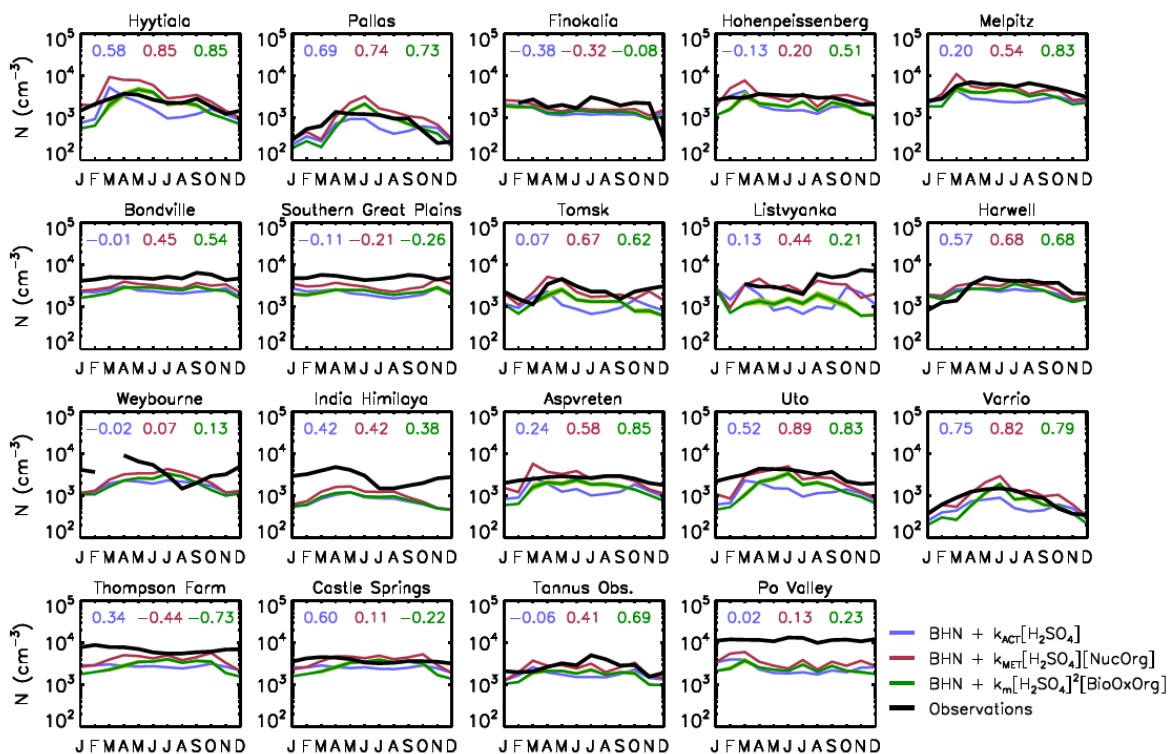


Figure 2. (A) Mass-defect plot of negative clusters measured by the APi-TOF and (B) the time series of the normalized concentration of growing clusters grouped in bands and the time series of the particle concentration measured with the DEG CPC with $D_{50} = 2$ nm and the CPC with $D_{50} = 3$ nm. Note that here the experiment was started by turning the electric clearing field off at 06:02, and the UV lights on at 06:11, so most of the observed growth (especially of the larger bands) is caused by formation of BioOxOrg, rather than by diffusional charging of already existing BioOxOrg. This is different from the experiments shown in 1B and 1C, where the sequence “neutral” \rightarrow “gr” \rightarrow “pion beam” was always followed. The clusters are grouped in bands, from 1 to 4, according to the number m of BioOxOrg molecules present in the clusters of band m . In the mass-defect plot the sulfuric acid monomers, dimers and trimers, $(\text{H}_2\text{SO}_4)_{0-2}\text{HSO}_4^-$, are shown in red. m oxidized organic molecules bound to HSO_4^- (1, m) are shown in yellow. m oxidized organic molecules bound to sulfuric acid dimers (2, m) and trimers (3, m) are shown in lighter and darker orange, respectively. In (A) the circle diameters are proportional to $(\text{count rates})^{1/2}$. The unidentified ions are shown in gray and nitrate-BioOxOrg clusters in dark violet. Water molecules evaporate rapidly in the APi-TOF and are not detected, as described in (28, 29, 33). The experimental conditions for this specific run were: $J = 4.38 \text{ cm}^{-3} \text{ s}^{-1}$, $[\text{H}_2\text{SO}_4] = 2.41 \cdot 10^6 \text{ cm}^{-3}$, $[\text{BioOxOrg}] = 3.81 \cdot 10^8 \text{ cm}^{-3}$, $T = 278 \text{ K}$, $\text{RH} = 39\%$.



5 **Figure 3.** Simulated and observed monthly mean total particle number concentration across 19 northern
 hemisphere continental boundary layer locations (11). Multi-annual observations, represented by the black
 line, are derived from measurements with minimum cut-off diameters ranging from 3 nm to 14 nm.
 Simulations using three different nucleation mechanisms are shown as colored lines: blue – BHN plus
 10 activation boundary layer nucleation (BHN + $k[H_2SO_4]$); red – BHN plus Metzger et al. (25) in the boundary
 layer; dark green – BHN plus the new mechanism (Eq. 2) in the boundary layer (see the SOM for a definition
 of these experiments). Light green shading around the dark green line for the new mechanism represents
 simulated particle concentrations at the edge of the 90% confidence interval for the value of k_m . Pearson
 correlation coefficient (R) given for each site (colored according to nucleation mechanism) at the top of each
 individual plot.

15